Neutron diffraction study of liquid Li_xSi_{1-x} alloys where x=0.80, 0.65 and 0.57

1995 J. Phys.: Condens. Matter 7 499

(http://iopscience.iop.org/0953-8984/7/3/006)

J. Phys.: Condens. Matter 7 (1995) 499–516. Printed in the UK

Neutron diffraction study of liquid Li_xSi_{1-x} alloys where $x = 0.80$, 0.65 and 0.57

P H K de Jong†¶, P Verkerk†, L A de Graaf†, W S Howells‡ and W van der Lugt§

† Interfaculty Reactor Institute, Delft University of Technology, Mekelweg 15, 2629 JB Delft, The Netherlands

‡ Rutherford Appleton Laboratory, Didcot, Oxon OX11 0QX, UK

§ Solid State Physics Laboratory, University of Groningen, 9747 AG Groningen, The Netherlands

Received 11 May 1994, in final form 27 October 1994

Abstract. We report a neutron diffraction experiment on liquid $^7Li_xSi_{1-x}$ alloys ($x = 0.80$, 0.65 and 0.57) just above the liquidus and on $^7Li_{57}Si_{43}$ at about 200 K above the liquidus. We obtained absolutely normalized and fully corrected structure factors and radial distribution functions, which provide indications for the occurrence of chemical ordering in all three alloys. We have analysed the data by fitting models to the structure factor and to the radial distribution function, and by using the reverse Monte Carlo (RMC) method. We find strong indications for the presence of covalently bonded Si in liquid $Li_{65}Si_{35}$ and $Li_{57}Si_{43}$. The Si–Si coordination number Z_{SiSi} varies from about 1.5 in $Li_{65}Si_{35}$ to about 2 in $Li_{57}Si_{43}$. For $c_{Si} > 0.2$, Si forms poly-anions ranging from dumbbells to large three-dimensional structures. Z_{SiSi} in $Li_{57}Si_{43}$ is not strongly temperature dependent and consequently the poly-anions are fairly stable. Covalently bonded Si is absent in liquid $Li_{80}Si_{20}$. The RMC modelling indicates that individual Si atoms are well separated. This suggests that the covalent character of Si in the Si-rich alloys ($Li_{65}Si_{35}$ and $Li_{57}Si_{43}$) changes to a more ionic character in $Li_{80}Si_{20}$.

1. Introduction

The Li–Si system belongs to the group of well studied alloys of alkali metals with post-transition group IV elements (see, e.g., Van der Lugt *et al* [1]). A large electronegativity difference between the constituents (e.g. 1.85 V for Li–Si, 1.30 V for Li–Sn and 1.25 V for Li–Pb [2]) gives rise to a charge transfer which is the cause of the deviation of the properties of these alloys from those of the pure elements. Li–Si deviates from the other lithium–post-transition group IV alloys Li–Ge, Li–Sn, Li–Pb: in the latter systems a sharp peak occurs in the resistivity and in the Knight shift as function of composition [3], whereas in liquid Li–Si a plateau in both properties has been observed by Meijer et al. [4]. In the discussion of their data Meijer *et al* assume that poly-anions are present in the liquid state and that precisely that number of covalent bonds is formed to keep the Fermi level at a minimum in the density of states. More hints for the structure of liquid Li–Si may be obtained from the structure in the solid phases. There are five intermediate phases (LiSi [5], $Li_{12}Si_7$ [6], $Li_{14}Si_6$ [7], $Li_{13}Si_4$ [8] and $Li_{21}Si_5$ [9]) in the solid state showing a rich variety of poly-anions (Si_2 dumbbells, Si_4 stars, Si_5 rings and three-dimensional networks).

¶ Present address: H H Wills Physics Laboratory, University of Bristol, Tyndall Avenue, Bristol BS8 1TL, UK.

0953-8984/95/030499+18$19.50

The density of liquid Li–Si alloys has been measured for Si concentrations between 20% and 43% using neutron transmission [10]. A volume contraction with respect to ideal mixing of up to 15% was observed, confirming the charge transfer assumed on the basis of the difference in electronegativity.

Recently De Wijs *et al* [11] performed *ab initio* molecular dynamics (AIMD) simulations on liquid $Li_{12}Si_7$ to study the atomic and electronic structures simultaneously. The AIMD simulation of liquid $Li_{12}Si_7$ [11] shows that the Fermi level is indeed in a minimum of the density of states. In the present paper we present neutron diffraction measurements on three liquid $^7Li_xSi_{1-x}$ alloys with $x = 0.80$, 0.65 and 0.57. $Li_{80}Si_{20}$ was chosen since it is in accordance with the simple chemical octet valence rule and it allows for a comparison with the other octet alloys of alkali metals with post-transition group IV elements. $Li_{65}Si_{35}$ is a zero alloy (the average coherent scattering length is zero), and hence we just measure the concentration–concentration fluctuation correlation. $Li_{57}Si_{43}$ was chosen because it corresponds to the eutectic composition. We could not measure at higher Si concentration, because then the temperature of the liquidus increases and the material (Ti–Zr) we used for the sample cell cannot be used at temperatures above 1073 K. It is not yet clear whether there is any suitable cell material for the Si-rich compositions ($c_{Si} > 0.43$) that will survive the high melting temperatures of these very aggressive alloys [12].

This paper is organized as follows. The experimental details are given in section 2. In section 3 the reduction of the experimental data is described. The results and the discussion are the subjects of section 4. A summary is given in the final section.

2. Experiment

The neutron diffraction experiment was performed with the Liquid and Amorphous materials Diffractometer (LAD) [13] at ISIS (Rutherford Appleton Laboratory, UK).

The sample cell, a cylinder made of the zero alloy $Ti_{67}Zr_{33}$, had an inner diameter of 14 mm, wall thickness 0.5 mm, and height 60 mm. We used lithium enriched in ^7Li because ^6Li strongly absorbs neutrons. The ^7Li specimen (enrichment 99.971 at.%) was obtained from Oak Ridge National Laboratory. We used high-purity (99.99%) Si of normal isotopic composition. The sample cells were filled in a helium-filled glovebox and sealed by means of laser beam welding through an evacuated glass tube. The compositions, relevant scattering lengths and cross-sections of the samples and the pure components are given in table 1. The beam size was 20×30 mm^2.

We performed measurements on liquid $Li_{80}Si_{20}$ at 973 K (for 13 hours), on $Li_{65}Si_{35}$ at 988 K (for 16 hours) and on $Li_{57}Si_{43}$ at 888 K and 1073 K (each for 11 hours). We repeatedly measured a vanadium rod of 8 mm diameter (for 16 hours in total), the empty cell at temperatures between 888 K and 1073 K (for 17 hours in total) and the empty furnace (for 5 hours in total). From an analysis of the multiply performed measurements we found that the stability of the monitors and the detectors was of the order of a few tenths of a per cent. The scattering from the empty cell and the furnace with respect to the scattering of the sample cells is typically in the order of 30–40% and 10–15%, respectively. The cells were slightly bent (a few degrees) after heating, which made an additional correction of the data necessary (see section 3).

Table 1. Compositions, relevant scattering lengths and cross-sections [14] of the samples and the pure components. n_s denotes the number density, H_s denotes the height of the sample in the cell and σ_s denotes the bound total scattering cross-section. The absorption cross-section (at 0.1 nm) used in the data analysis is denoted by σ_a, $\langle\bar{b}\rangle$ and $\langle\bar{b}^2\rangle$ denote the coherent scattering length and the mean squared coherent scattering length, respectively.

Composition	T /K	n_s /nm^{-3}	H_s /mm	σ_a /b	σ_s /b	$\langle\bar{b}\rangle$ /fm	$\langle\bar{b}^2\rangle$ /b
^{7}Li (99.971 at.%)					1.30	−0.222	
Si					2.178	0.4149	
$Li_{0.7999}Si_{0.2001}$	973	50.4	45.3	0.310	1.48		0.0740
$Li_{0.6501}Si_{0.3499}$	988	53.6	39.3	0.281	1.61		0.0923
$Li_{0.5693}Si_{0.4307}$	888	56.2	30.2	0.244	1.68		0.102
$Li_{0.5693}Si_{0.4307}$	1073	54.0	31.5	0.245	1.68		0.102

3. Data reduction

The experimental data were corrected for background, dead time, detector efficiency, multiple scattering, self-shielding and inelasticity, and normalized using the ATLAS analysis programs (Soper *et al* [15]). The data were not corrected for resolution because the widths of the sharpest peaks are much broader than the width of the resolution. In this section we will pay attention to steps where problems occurred, or that are otherwise worth discussing.

For a number of corrections (e.g. for multiple scattering) the total cross-section $\sigma(\lambda)$ as function of the neutron wavelength λ is required. This quantity is related to the *a priori* unknown factor $S(\kappa)$ (see, e.g., equation (2.4.1) in [15]). $\sigma(\lambda)$ for each alloy is calculated from the experimental data on the transmission of the sample. The experimental $\sigma(\lambda)$ for $Li_{80}Si_{20}$ at small λ is unphysical for unknown reasons. Therefore we have calculated $\sigma(\lambda)$ for $Li_{80}Si_{20}$ by using the value for the total cross-section in the short-wavelength limit and the absorption cross-section which was determined from a fit to the experimental data for $0.15 \leqslant \lambda \leqslant 0.3$ nm. We applied the whole correction procedure using the experimental $\sigma(\lambda)$. The fully corrected structure factor and the experimentally determined absorption cross-section have been used to calculate a new $\sigma(\lambda)$ in order to check whether the original $\sigma(\lambda)$ was correct. From the smallness of the difference between the two results for $\sigma(\lambda)$ we conclude that a second iteration through the data correction is not necessary.

The correction for inelastic effects is large for liquids containing light elements, in particular lithium and (to a lesser extent) silicon. We applied the second-order Placzek correction [16] in the usual way to only $(d\sigma/d\Omega)_s$, the self-part of the differential cross-section $d\sigma/d\Omega$, assuming that the correction to the distinct part is small enough to be neglected. The correction diverges at small κ and is fairly independent of κ over a large κ-range. Consequently, the data can only be used beyond a minimum κ (different for each detector position) because of the uncertainty in the inelasticity correction.

The experimentally determined differential cross-sections $(d\sigma/d\Omega)_{exp}$ in the large-κ limit (about 150–250 nm^{-1}) differ from the expected values of $\sigma_s/(4\pi)$ with σ_s the total scattering cross-section. The mean ratio between $(d\sigma/d\Omega)_{exp}$ and $\sigma_s/(4\pi)$, averaged over the detectors used, for $Li_{80}Si_{20}$, $Li_{65}Si_{35}$, $Li_{57}Si_{43}$ at 888 K and $Li_{57}Si_{43}$ at 1073 K is 1.137(17), 1.115(16), 1.238(18) and 1.407(24), respectively. The deviations from unity are apparent and indicate that the data are badly normalized. The small standard deviations ($\approx$1%) are consistent with the results of our assessment of the stability (see section 2) and indicate that the drift in individual detectors is low. Verkerk *et al* [10] observed that liquid Li–Si alloys

strongly adhere to the walls of the cell. The normalization errors are therefore probably due to the fact that the irradiated part of the cell was not completely filled with the sample. Consequently, we have renormalized our data with respect to $\sigma_s/4\pi$.

We noticed a shift in κ when we plotted the spectra from adjacent detectors in the same figure. This is most probably the result of the bending of the sample cells (see section 2). By trial and error we determined an effective scattering angle for the detectors at the two smallest scattering angles (5° and 10°) to take this effect into account. The scattering angles of the adjacent detectors at 20° were not altered because we did not observe deviations from the detectors at larger angles where the effect of a displacement is negligible. The differences between the original scattering angles at 5° and 10° and the scattering angles determined using this procedure were less than 0.2°. This corresponds to a displacement of the sample cell of a few mm. We do not find a consistent displacement for one sample. A possible explanation is that the original angles of the detectors were incorrect.

We combined data from different detectors by applying the standard method [15] to determine a region of overlap between successive detectors using the intensities of the vanadium measurements as a weighting function. We only use neutrons with a wavelength smaller than 0.11 nm because of the uncertainty in the inelasticity correction.

4. Results and discussion

4.1. Structure factors

The static structure factor $S(\kappa)$ in terms of the Ashcroft–Langreth (AL) partial structure factors S_{ij} [17] is

$$S(\kappa) = w_{11}S_{11}(\kappa) + w_{12}S_{12}(\kappa) + w_{22}S_{22}(\kappa)$$

with the weight factors

$$w_{11} = \frac{c_1\overline{b}_1^2}{\langle\overline{b}^2\rangle} \qquad w_{12} = \frac{2\sqrt{c_1c_2}\,\overline{b}_1\overline{b}_2}{\langle\overline{b}^2\rangle} \qquad w_{22} = \frac{c_2\overline{b}_2^2}{\langle\overline{b}^2\rangle}$$

where $\overline{b}_i$ and c_i denote the coherent scattering length and concentration of species i, respectively. In the following we use index 1 for Li and index 2 for Si. The AL weight factors w_{ij} for the three Li–Si alloys are listed in table 2.

Table 2. Weight factors for the Ashcroft–Langreth and Bhatia–Thornton partial structure factors for $Li_{80}Si_{20}$, $Li_{65}Si_{35}$ and $Li_{57}Si_{43}$.

	Ashcroft–Langreth			Bhatia–Thornton		
	w_{11}	w_{12}	w_{22}	w_{NN}	w_{NC}	w_{CC}
$Li_{80}Si_{20}$	0.533	−0.996	0.465	0.121	1.63	5.48
$Li_{65}Si_{35}$	0.347	−0.952	0.653	0.000	−0.0126	4.40
$Li_{57}Si_{43}$	0.275	−0.894	0.726	0.0264	−0.648	3.98

$S(\kappa)$ of a binary alloy can also be written as

$$S(\kappa) = w_{NN}S_{NN}(\kappa) + w_{NC}S_{NC}(\kappa) + w_{CC}S_{CC}(\kappa).$$

$S_{CC}(\kappa)$, $S_{NC}(\kappa)$, and $S_{NN}(\kappa)$ are the Bhatia–Thornton (BT) partial structure factors [18] which describe the structure in terms of concentration C and particle number density N.

$S_{CC}(\kappa) \to c_1c_2$ for $\kappa \to \infty$. $S_{CC}(\kappa) = c_1c_2$ if the atoms are randomly distributed. The weight factors for the BT partial structure factors (see table 2) are

$$w_{NN} = \frac{\langle\bar{b}\rangle^2}{\langle\bar{b}^2\rangle} \qquad w_{NC} = 2\frac{\langle\bar{b}\rangle\,\Delta\bar{b}}{\langle\bar{b}^2\rangle} \qquad w_{CC} = \frac{(\Delta\bar{b})^2}{\langle\bar{b}^2\rangle}$$

where $\langle\bar{b}\rangle = c_1\bar{b}_1 + c_2\bar{b}_2$ is the mean coherent scattering length and $\Delta\bar{b} = \bar{b}_1 - \bar{b}_2$. $S(\kappa)$ of a zero alloy is equal to $S_{CC}(\kappa)/c_1c_2$ since $\langle\bar{b}\rangle = 0$ and $w_{CC} = 1/c_1c_2$.

Analogously to conventional coordination numbers one could define a C–C coordination number Z_{CC} [19]:

$$Z_{CC} = 4\pi n_s \int_0^{R_{CC}} r^2 g_{CC}\,\mathrm{d}r \tag{1}$$

with

$$g_{CC}(r) = \frac{1}{2\pi^2 n_s r}\int_0^{\infty} \kappa\left(\frac{S_{CC}}{c_1c_2} - 1\right)\sin(\kappa r)\,\mathrm{d}\kappa \tag{2}$$

where R_{CC} is the outer radius of the first coordination shell of $g_{CC}(r)$ and n_s denotes the number density.

Z_{CC} can be expressed in terms of Z_{ij}, the coordination number of atoms of species j around an atom of species i

$$Z_{CC} = Z_W - Z_{12}/c_2 = Z_W - Z_{21}/c_1 \tag{3}$$

where the number of nearest neighbours $Z_W = c_2Z_1 + c_1Z_2$ and Z_i is $Z_{i1} + Z_{i2}$. Harris and Lewis [20] define a generalized Warren chemical short-range order (CSRO) parameter α_W as

$$\alpha_W = Z_{CC}/Z_W. \tag{4}$$

For a random system $Z_{ij} = c_jZ_i$, yielding $\alpha_W = 0$. For a system with a preference for a hetero- (self-) coordination α_W is negative (positive) [20].

In figure 1 we show the fully corrected $S(\kappa)$.. All three Li–Si alloys show strong chemical ordering since the $S(\kappa)$s of these alloys (equal to or dominated by $S_{CC}(\kappa)$) show oscillations up to large κ. Two peaks occur between 30 and 45 nm^{-1} in $S(\kappa)$ of $Li_{80}Si_{20}$ and $Li_{65}Si_{35}$. The first of these two peaks in $Li_{65}Si_{35}$ is significantly larger than in $Li_{80}Si_{20}$. At $Li_{57}Si_{43}$ these two peaks merge together. In figure 2 we show $S(\kappa)$ at large κ-values on an expanded scale. We observe oscillations for κ beyond 100 nm^{-1} in $Li_{65}Si_{35}$ and $Li_{57}Si_{43}$, and the oscillations in $Li_{57}Si_{43}$ at 888 K extend out to 180 nm^{-1}. These oscillations reflect one or more well defined intramolecular distances in the liquid state. We have fitted the data for $Li_{65}Si_{35}$ and $Li_{57}Si_{43}$ at 888 K and 1073 K at large κ ($100 \leqslant \kappa \leqslant 140$ nm^{-1}) with an intramolecular form factor $F_{\mathrm{intra}}(\kappa)$ (see e.g. [21] or [22])

$$F_{\mathrm{intra}}(\kappa) = p + t\frac{\sin(\kappa L)}{\kappa L}\exp(-\langle u^2\rangle\kappa^2/2) \tag{5}$$

where both p and t are normalization constants, L denotes the intramolecular distance and $\langle u^2\rangle$ is the mean square amplitude of vibration.

The weighted RMSE (the square root of the sum of squares divided by the number of degrees of freedom) was less than one in all three cases. The $Li_{80}Si_{20}$ data were fitted in a different way (see below) because the oscillations at large κ are very weak. The results are given in table 3. The fitting parameters t and $\langle u^2\rangle$ are strongly correlated.

We find that the data at large κ-values are well described with an intramolecular form factor using a single intramolecular distance. The fitted intramolecular distance agrees well

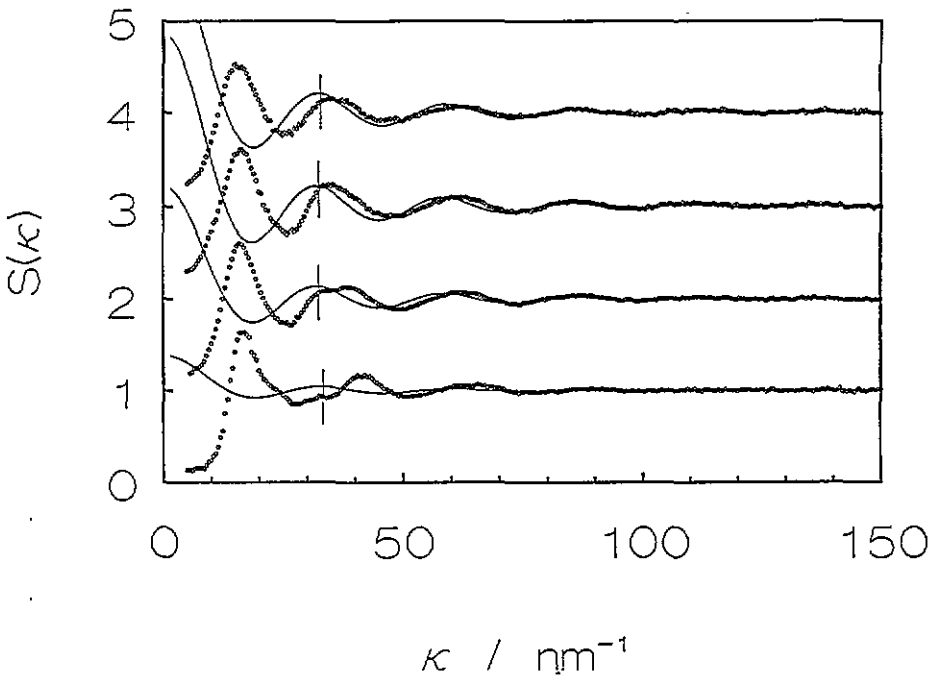

Figure 1. Fully corrected $S(\kappa)$ for $Li_{80}Si_{20}$ at 973 K, $Li_{65}Si_{35}$ at 988 K (ordinate shifted by +1.0), $Li_{57}Si_{43}$ at 888 K (ordinate shifted by +2.0) and $Li_{57}Si_{43}$ at 1073 K (ordinate shifted by +3.0). Circles: experimental results; solid lines: intramolecular form factor; vertical line: second maximum of the intramolecular form factor.

Table 3. Results of the analysis of the large-κ part of $S(\kappa)$ using an intramolecular form factor. The quantities p, t, L and $\langle u^2 \rangle$ are described in the text. Z_{SiSi} denotes the average number of Si anions in the first coordination shell of a Si anion.

Composition	p	L/nm	$\langle u^2 \rangle$/nm^2	t	Z_{SiSi}
$Li_{65}Si_{35}$	1.01	0.237	1.72×10^{-4}	1.10	
$Li_{57}Si_{43}$ at 888 K	1.01	0.240	2.82×10^{-4}	3.28	
$Li_{57}Si_{43}$ at 1073 K	1.01	0.236	1.80×10^{-4}	1.81	
with $\langle u^2 \rangle = 1.76 \times 10^{-4}$ nm^2 and $p = 1.0$:					
$Li_{80}Si_{20}$		0.234		0.4(2)	0.8(4)
$Li_{65}Si_{35}$		0.240		1.2(3)	1.8(5)
$Li_{57}Si_{43}$ at 888 K		0.241		1.9(7)	2.5(9)
$Li_{57}Si_{43}$ at 1073 K		0.237		1.8(9)	2.4(1.2)

with the distance between covalently bonded Si in solid $Li_{12}Si_7$ (0.236–0.238 nm) [6], solid $Li_{14}Si_6$ (0.234 nm) [7] and solid LiSi (0.242 and 0.250 nm) [5]. The fitted intramolecular distance is smaller than the smallest Li–Si and Li–Li distances in the solid state. The Si–Si partial pair correlation function $g_{SiSi}(r)$ in AIMD simulations of liquid KSi [23] and liquid $Li_{12}Si_7$ [11], has a sharp peak at a similar short distance (0.24 nm and 0.245 nm, respectively). A small Li–Li distance is not very likely because of the charge transfer due to the large difference in electronegativity. We therefore assume that the oscillations at large κ in $S(\kappa)$ are due to a well-defined intramolecular distance between Si atoms.

The value of $\langle u^2 \rangle$ in $Li_{57}Si_{43}$ at 888 K is about 50% larger than the value of $\langle u^2 \rangle$ of $Li_{57}Si_{43}$ at 1073 K. This appears to be compensated by a strong increase of the value of

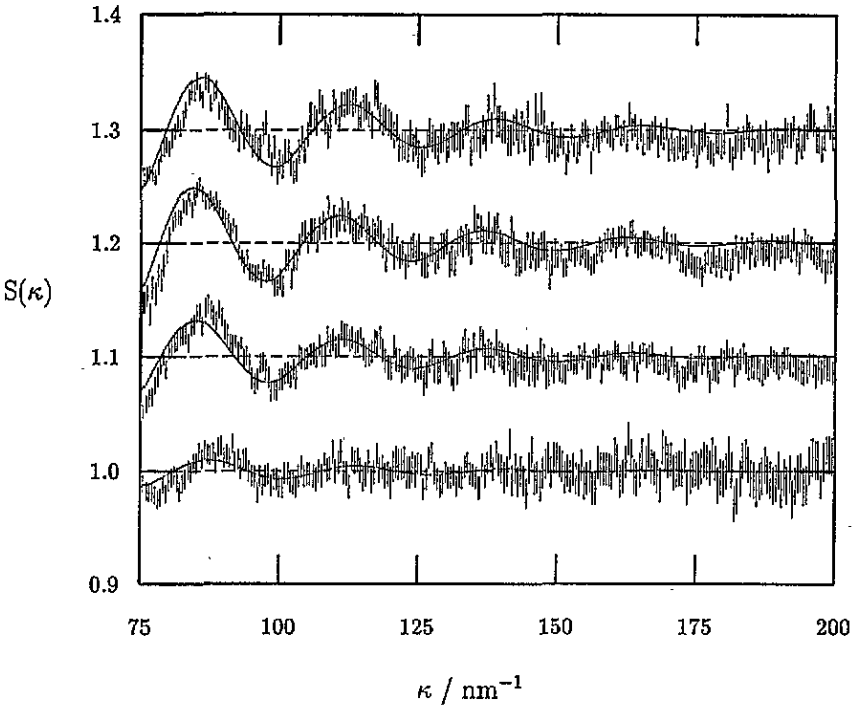

Figure 2. Fully corrected $S(\kappa)$ for $Li_{80}Si_{20}$ at 973 K, $Li_{65}Si_{35}$ at 988 K (ordinate shifted by +0.1), $Li_{57}Si_{43}$ at 888 K (ordinate shifted by +0.2) and $Li_{57}Si_{43}$ at 1073 K (ordinate shifted by +0.3). Solid lines: intramolecular form factor.

t. We use the width of the first peak of $g_{SiSi}(r)$ from AIMD simulations for liquid $Li_{12}Si_7$ at 1050 K (2.30×10^{-4} nm^2) [11] and liquid KSi at 1050 K (2.10×10^{-4} nm^2) [23] as an estimate of $\langle u^2 \rangle$. For comparison, $\langle u^2 \rangle$ in solid $Li_{12}Si_7$ [6] and solid $Li_{14}Si_6$ [8] is 1.30×10^{-4} nm^2 and 1.70×10^{-4} nm^2, respectively.

In order to reduce the number of free parameters we fixed $\langle u^2 \rangle$ at the average of the fitted values for $Li_{65}Si_{35}$ and $Li_{57}Si_{43}$ at 1073 K and we fixed p at unity during the remaining analysis. The same model with fixed $\langle u^2 \rangle$ (1.76×10^{-4} nm^2) and p was then fitted to all four $S(\kappa)$s for $100 \leqslant \kappa \leqslant 140$ nm^{-1}. The fitted curves are indicated in figures 1 and 2, and the fitting parameters are listed in table 3. We note the following. (i) The RMSE remained less than unity in all cases. (ii) The position of the second maximum of the intramolecular form factor (see figure 1) is very close to the position of the first of the two peaks at 30–45 nm^{-1} in $Li_{65}Si_{35}$ and $Li_{80}Si_{20}$. (iii) $S(\kappa)$ for $Li_{80}Si_{20}$, in contrast to $S(\kappa)$ for $Li_{65}Si_{35}$ and $Li_{57}Si_{43}$, does not deviate from unity for κ between 100 and 140 nm^{-1}.

We estimate the Si–Si coordination number Z_{SiSi} from the area of the Fourier transform of equation (5) using the values of the parameters after fitting. The results are given in table 3. The large uncertainty in Z_{SiSi} reflects the strong correlation between t and $\langle u^2 \rangle$. We find that Z_{SiSi} strongly increases at increasing Si concentration. The same occurs in the solid state where Z_{SiSi} increases from 1 in $Li_{14}Si_6$ [7] to 1.86 in $Li_{12}Si_7$ [6] and 3 in LiSi [5].

4.2. Pair correlation functions

The pair correlation functions $g(r)$, where

$$g(r) = \frac{1}{2\pi^2 n_s r}\int_0^\infty \kappa(S(\kappa)-1)\sin(\kappa r)\,\mathrm{d}\kappa$$

were obtained via a direct Fourier transform of $S(\kappa)$s (using the standard program available in the ATLAS analysis programs). We define $g(r)$ in this way because $g(r)$ of the zero alloy $Li_{65}Si_{35}$ yields directly $g_{CC}(r)$ (see equation (2)). $g(r)$ in terms of the AL partial pair correlation functions $g_{ij}(r)$ is

$$g(r) = \frac{c_1^2\bar{b}_1^2}{\langle\bar{b}^2\rangle}g_{11}(r) + \frac{2c_1c_2\bar{b}_1\bar{b}_2}{\langle\bar{b}^2\rangle}g_{12}(r) + \frac{c_2^2\bar{b}_2^2}{\langle\bar{b}^2\rangle}g_{22}(r) - \frac{\langle\bar{b}\rangle^2}{\langle\bar{b}^2\rangle}. \tag{6}$$

Note that $g(r) \to 0$ when $r \to \infty$. In figure 3 we show the results for $g(r)$. The interatomic distances occurring in the adjacent solid-state phases are also indicated; the relation with the solid state is evident. The most remarkable feature of these pair correlation functions is the coincidence of the first maximum in $g(r)$ of $Li_{65}Si_{35}$ and $Li_{57}Si_{43}$ with the distance between covalently bonded Si in solid Li–Si alloys. The positive peak at the distance where covalently bonded Si occurs in the solid state is absent in $g(r)$ of $Li_{80}Si_{20}$ (see arrow in figure 3).

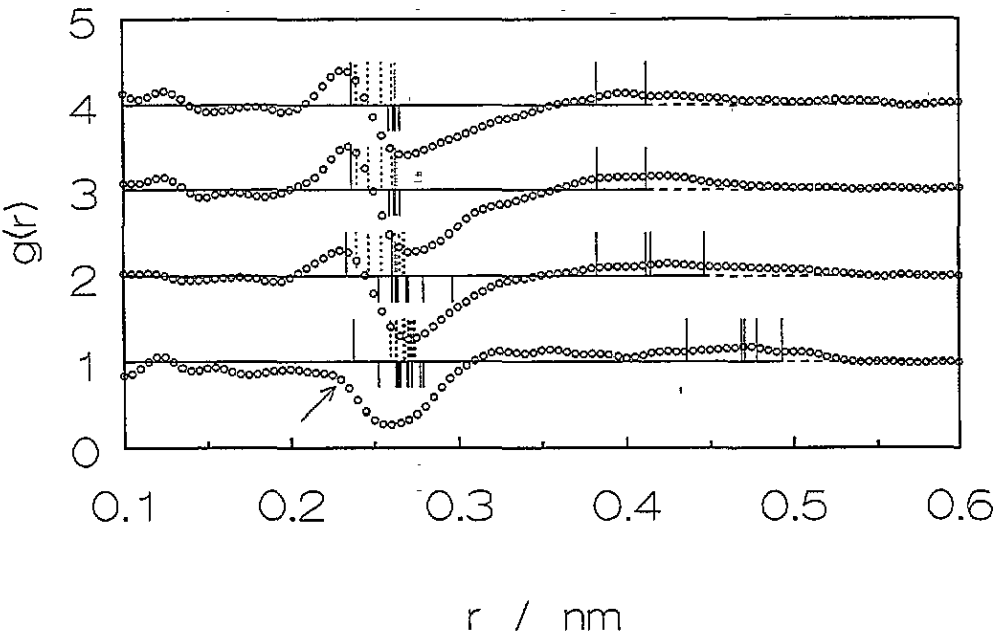

Figure 3. Pair correlation functions (circles) for $Li_{80}Si_{20}$ (ordinate shifted by + 1.0), $Li_{65}Si_{35}$ (ordinate shifted by + 2.0), $Li_{57}Si_{43}$ at 888 K (ordinate shifted by + 3.0) and $Li_{57}Si_{43}$ at 1073 K (ordinate shifted by + 4.0). Only the first few solid-state distances (see [6], [7], [8], [9] and [30]) are given. Positive solid lines: Si–Si; negative solid lines: Li–Si; positive dotted lines: Li–Li. Note that the positive solid line in $g(r)$ of $Li_{80}Si_{20}$ corresponds to the Si–Si distance in $Li_{13}Si_4$ (=$Li_{76}Si_{24}$). The arrow in $g(r)$ of $Li_{80}Si_{20}$ denotes the position where the positive peak occurs in the other Li–Si alloys.

We obtain $S_{CC}(\kappa)$ for $Li_{80}Si_{20}$ and $Li_{57}Si_{43}$ approximately by neglecting the contributions from $S_{NN}(\kappa)$ and $S_{NC}(\kappa)$ (see table 2). The first peak in $g(r)$ for $Li_{65}Si_{35}$ and

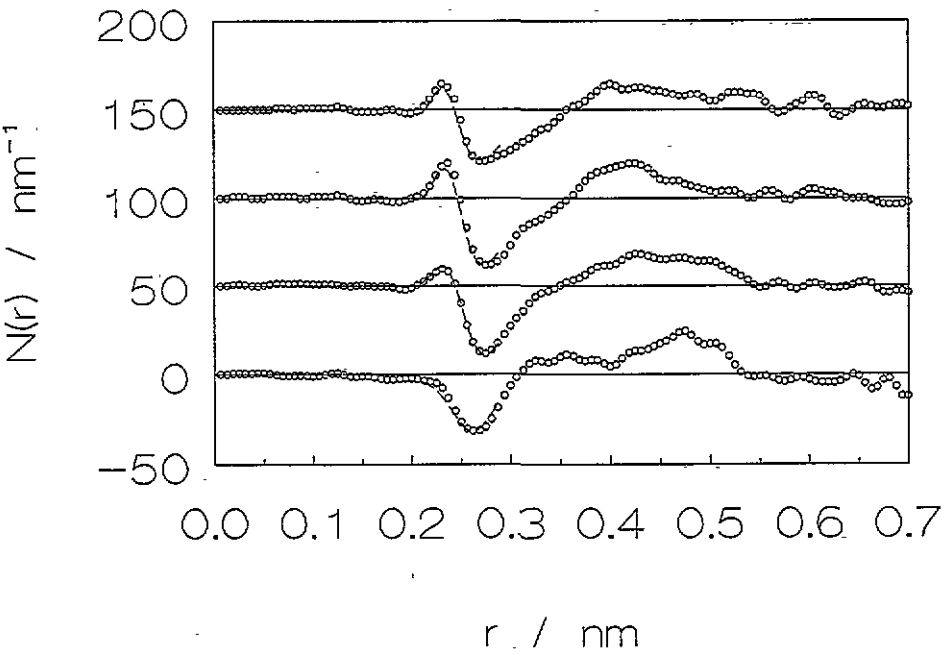

Figure 4. Radial distribution functions for $Li_{80}Si_{20}$, $Li_{65}Si_{35}$ (ordinate shifted by +50), $Li_{57}Si_{43}$ at 888 K (ordinate shifted by +100) and $Li_{57}Si_{43}$ at 1073 K (ordinate shifted by +150). Broken lines: fitted model.

$Li_{57}Si_{43}$ indicates a preference for self-coordination because the area of the peak is positive (see section 4.1). The first minimum reflects a hetero-coordination since it has a negative area. The minimum in $Li_{80}Si_{20}$ again indicates a preference for a hetero-coordination.

In figure 4 we show the radial distribution functions $N(r)$ ($=4\pi r^2 n_s g(r)$). We have fitted $N(r)$ over a limited r-range (from 0.2 to 0.3 nm) with a sum of two Gaussians (only one for $Li_{80}Si_{20}$) in order to determine interatomic distances and partial coordination numbers. We use the following model:

$$N(r) = \sum_{i=1}^{2} a_i \frac{1}{s_i\sqrt{2\pi}} \exp\left(\frac{(r-d_i)^2}{2s_i^2}\right) - 4\pi r^2 n_s \frac{\langle\bar{b}\rangle^2}{\langle\bar{b}^2\rangle}$$

where a_i, s_i and d_i denote the amplitudes, the standard deviations and the positions of the Gaussians, respectively. The results of the fits for 0.2 nm $\leqslant r \leqslant$ 0.3 nm are given in table 4. The fitted curves are also given in figure 4. The distances d_1 of the Si-rich alloys $Li_{65}Si_{35}$ and $Li_{57}Si_{43}$ are in reasonable agreement with the distances determined from a fit with an intramolecular form factor to the large-κ part of $S(\kappa)$ (see table 3).

We determined Z_{SiSi} from the area of the first peak of $Li_{65}Si_{35}$ and $Li_{57}Si_{43}$ under the assumption that this peak is due only to a Si–Si contribution. Z_{SiSi} (table 4) is given by the ratio of a_1 and $c_2\bar{b}_2^2/\langle\bar{b}^2\rangle$ (see equation (6)). The results are in reasonable agreement with the results of the analysis of $S(\kappa)$ with an intramolecular form factor. The small reduction of Z_{SiSi} in $Li_{57}Si_{43}$ at increasing temperatures indicates that the poly-anions do not dissociate.

We have calculated the number of Si atoms surrounding a Li atom, Z_{LiSi}, from $N(r)$ by using equation (3). In this calculation we use the areas of the two fitted Gaussians (see table 4) to determine Z_{CC} and we assume that each atom has ten nearest neighbours (Z_W). Note that this is an approximation for $Li_{80}Si_{20}$ and $Li_{57}Si_{43}$ because we neglect the contributions

Table 4. Results of the fits to the radial distribution functions, the results of the RMC analysis and the analysis in terms of an intramolecular form factor. a_i, d_i and s_i are the parameters of the fitted Gaussians. For the determination of Z_{LiSi} and Z_{SiSi} of the RMC configurations we used 0.35 nm and 0.28 nm respectively as r_{max}, the outer diameter of the first coordination shell. Z_{LiSi} in a random configuration was calculated using the number of nearest neighbours determined from the RMC configurations with $r_{max} = 0.35$ nm. The uncertainty in Z_{LiSi} and Z_{SiSi} includes the effect of using different values for r_{max}.

	$Li_{80}Si_{20}$	$Li_{65}Si_{35}$	$Li_{57}Si_{43}$ at 888 K	$Li_{57}Si_{43}$ at 1073 K
a_1		1.07	1.27	1.11
d_1/nm		0.238	0.237	0.235
s_1/nm		0.0151	0.0136	0.0136
a_2	−1.33	−2.78	−2.68	−2.30
d_2/nm	0.261	0.270	0.268	0.261
s_2/nm	0.0198	0.0271	0.0281	0.0314

	Z_{LiSi}			
	$Li_{80}Si_{20}$	$Li_{65}Si_{35}$	$Li_{57}Si_{43}$ at 888 K	$Li_{57}Si_{43}$ at 1073 K
From $N(r)$	2.3(2)	4.1(4)	4.9(6)	4.9(4)
From RMC	2.4(2)	4.0(5)	5.0(6)	4.7(6)
Random	1.9	3.4	4.2	4.0

	Z_{SiSi}			
	$Li_{80}Si_{20}$	$Li_{65}Si_{35}$	$Li_{57}Si_{43}$ at 888 K	$Li_{57}Si_{43}$ at 1073 K
From $S(\kappa)$	0.8(4)	1.8(5)	2.5(9)	2.4(1.2)
From $N(r)$	—	1.7(5)	1.8(5)	1.5(3)
From RMC	0.10(5)	1.4(1)	2.0(1)	1.9(1)

from $S_{NN}(\kappa)$ and $S_{NC}(\kappa)$. The results are listed in table 4.

4.3. RMC *modelling*

In order to extract more information from the present data we used the reverse Monte Carlo method [24]. This method yields a three-dimensional configuration with an $S(\kappa)$ which is consistent with the experimental data. The results for $Li_{65}Si_{35}$ and $Li_{57}Si_{43}$ at 888 K and 1073 K have been reported elsewhere [25, 26]. Firstly, we will summarize the results of the RMC modelling of $Li_{65}Si_{35}$ and $Li_{57}Si_{43}$ at 888 K and at 1073 K. Secondly, we will pay attention to the RMC modelling of $Li_{80}Si_{20}$. Finally, we will compare the RMC results with the results of the data analysis by fitting models to $S(\kappa)$ and to $N(r)$.

We used four starting configurations for the RMC modelling of $Li_{65}Si_{35}$ and $Li_{57}Si_{43}$ at 888 K and at 1073 K, namely two random configurations and two configurations that resemble the solid-state phases whose compositions are closest to those of the liquid alloy under investigation. A comparison of the experimental $S(\kappa)$s and the RMC $S(\kappa)$s is given in figure 5. The RMC $S(\kappa)$s are in good agreement with the experimental $S(\kappa)$s. In figure 6 we show the results of the RMC modelling of the Li–Si alloys for the partial pair correlation functions. $g_{SiSi}(r)$ has a very sharp peak and a low first minimum. The position of the peak is close to the distance between covalently bonded Si in the solid state. Z_{SiSi} varies from about 1.4 in $Li_{65}Si_{35}$ to 2.0 (1.9) in $Li_{57}Si_{43}$ at 888 K (1073 K). We do not find Si_4 stars and Si_5 rings in the RMC configurations representing liquid $Li_{65}Si_{35}$ and $Li_{57}Si_{43}$. Si is

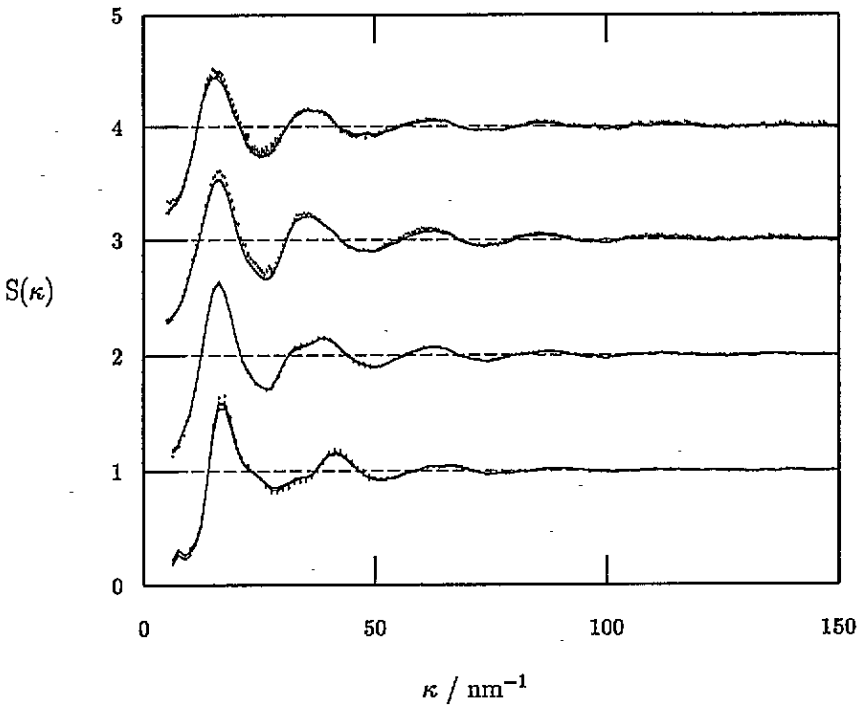

Figure 5. Comparison of the experimental $S(\kappa)$s with the RMC $S(\kappa)$s for $Li_{80}Si_{20}$, $Li_{65}Si_{35}$ (ordinate shifted by +1), $Li_{57}Si_{43}$ at 888 K (ordinate shifted by +2) and $Li_{57}Si_{43}$ at 1073 K (ordinate shifted by +3). Dots with arrow bars: experimental $S(\kappa)$; solid lines: RMC $S(\kappa)$s.

present in a variety of poly-anions ranging from isolated Si atoms to large three-dimensional clusters.

We adopted a similar approach for the RMC modelling of $Li_{80}Si_{20}$. We used three starting configurations, two random configurations (3000 atoms) and one configuration (1800 atoms) that resembles $Li_{13}Si_4$. The closest distances of approach (Li–Li: 0.240 nm, Li–Si: 0.230 nm, Si–Si: 0.220 nm) were again smaller than the interatomic distances in the intermediate phases $Li_{21}Si_5$ and $Li_{13}Si_4$. In figure 5 we also show the experimental and the RMC $S(\kappa)$s for $Li_{80}Si_{20}$. The two $S(\kappa)$s for $Li_{80}Si_{20}$ are in good agreement apart from minor deviations near the first maximum and first minimum of $S(\kappa)$.

The partial pair correlation functions for $Li_{80}Si_{20}$ are given in figure 6. The most remarkable feature of $g_{SiSi}(r)$ of $Li_{80}Si_{20}$ with respect to $g_{SiSi}(r)$ of the other alloys is the absence of the peak at about 0.237 nm. $g_{SiSi}(r)$ has a broad maximum at a distance which is close to the mean separation distance between Si atoms (0.52 nm). This distance was calculated by considering the Si atoms as hard spheres at close packing. Only a small spike at about 0.22 nm remains in $g_{SiSi}(r)$ of $Li_{80}Si_{20}$. The RMC fitting to $S(\kappa)$ is not very sensitive to such a spike because the Fourier transform of this spike is a very weak and broad contribution in κ-space. This is confirmed by an RMC fit to one of the configurations where we used a larger closest distance of approach for Si (0.25 nm). The $g_{LiLi}(r)$ of the three configurations differ from one another and the first peak of $g_{LiLi}(r)$ is broad. The Li–Li coordination number is therefore not well defined. $g_{LiSi}(r)$ in $Li_{80}Si_{20}$ is very sharp and the position of the first peak coincides with the first few interatomic distances between Li and Si in $Li_{21}Si_5$ and $Li_{13}Si_4$.

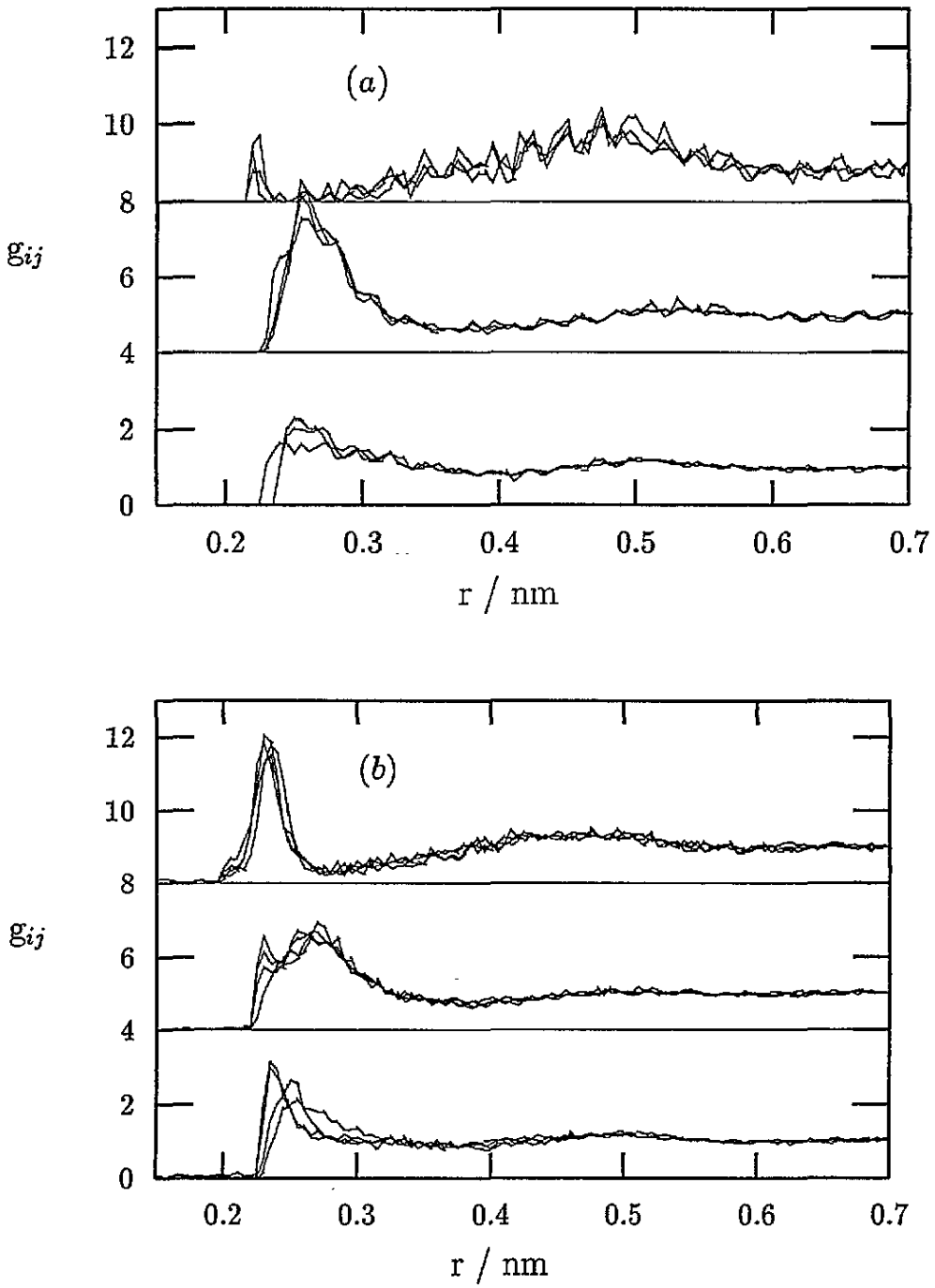

Figure 6. RMC results for the partial pair correlation functions $g_{LiLi}(r)$, $g_{LiSi}(r)$ (ordinate shifted by +4) and $g_{SiSi}(r)$ (ordinate shifted by +8) as resulting from different starting configurations for $Li_{80}Si_{20}$ (*a*), $Li_{65}Si_{35}$ (*b*), $Li_{57}Si_{43}$ at 888 K (*c*) and $Li_{57}Si_{43}$ at 1073 K (*d*).

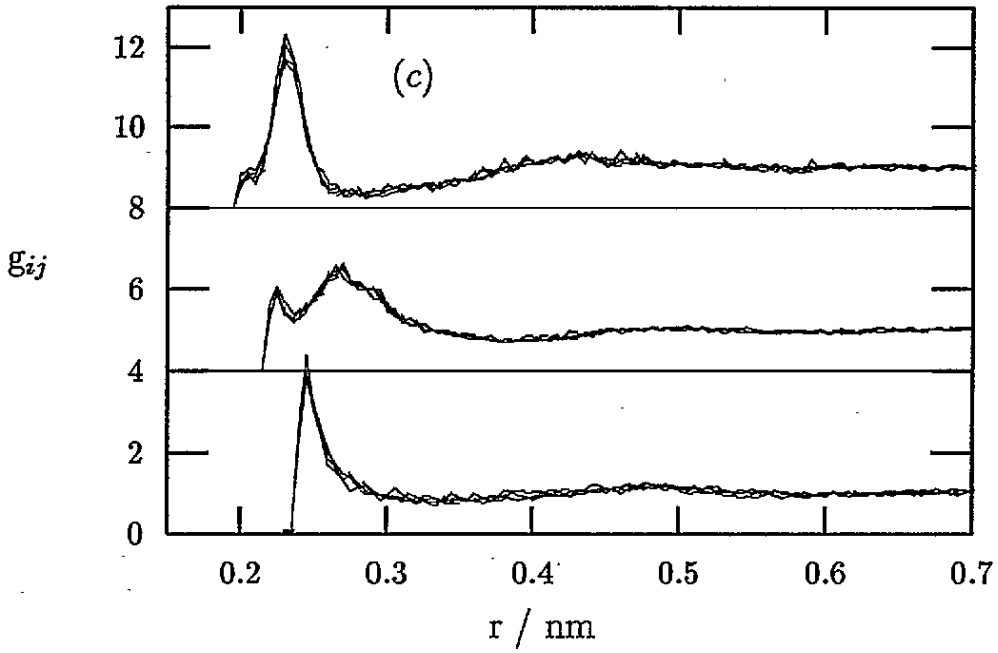

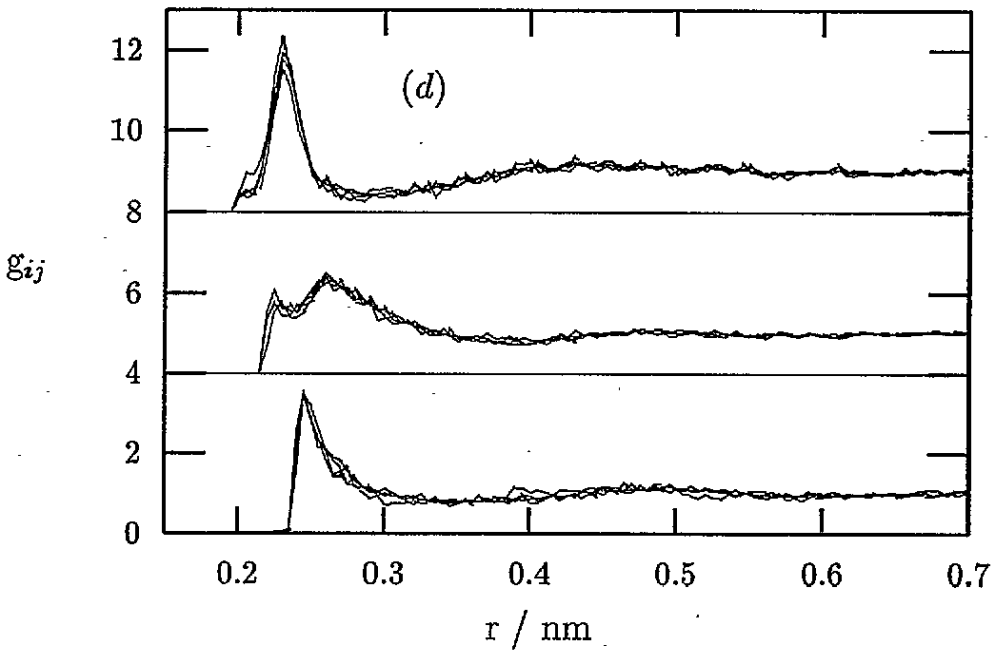

Figure 6. *Continued.*

We calculated Z_{LiSi} from $g_{LiSi}(r)$ up to 0.35 nm for all three alloys (see table 4). Z_{LiSi} varies from 2.4 in $Li_{80}Si_{20}$ to about 5 in $Li_{57}Si_{43}$. The accuracy of Z_{LiSi} was estimated from the results of the different configurations using different values for r_{max}, the outer radius of the coordination shell (0.33–0.37 nm). Z_{LiSi} of solid $Li_{21}Si_5$, $Li_{13}Si_4$, $Li_{14}Si_6$ and $Li_{12}Si_7$ is 3.1, 3.7, 5.2 and 4.7, respectively if we use $r_{max} = 0.35$ nm. Hence a similar increase of Z_{LiSi} at increasing Si concentration also occurs in the solid state. In table 4 we list Z_{LiSi} determined from $N(r)$. Z_{LiSi} was extracted from $N(r)$ under the assumption that $Z_W = 10$. This number is close to the values determined from the RMC configurations. For $Li_{80}Si_{20}$, $Li_{65}Si_{35}$ and $Li_{57}Si_{43}$ at 888 K and 1073 K we find 9.5, 9.6, 9.7 and 9.3 nearest neighbours respectively if we use $r_{max} = 0.35$ nm. This allows us to make a direct comparison between Z_{LiSi} determined from $N(r)$ and Z_{LiSi} determined from the RMC modelling. The Z_{LiSi} determined using these two methods are in good agreement and they differ by about 15–20% from $Z_{LiSi,r}$ in a random configuration, where $Z_{LiSi,r} = c_2$ times the number of nearest neighbours (see table 4), for the same r_{max}. A similar deviation occurs in liquid Li_4Pb where this difference is about 25%. The value of Z_{LiSi} in an AIMD simulation of liquid $Li_{12}Si_7$ [11] varies from 4.3 for an upper limit of the integration range of 0.34 nm to 4.9 for an upper limit of 0.38 nm. This is in good agreement with our results.

We have determined Z_{SiSi} in three ways. By fitting models to $S(\kappa)$ and to $N(r)$, and by using the RMC method. The results are listed in table 4. We use 0.28 nm as the outer radius of the first Si–Si coordination shell for the determination of Z_{SiSi} from the RMC configurations because this distance corresponds to the first minimum of $g_{SiSi}(r)$ in the Si-rich alloys. The accuracy of Z_{SiSi} from the RMC modelling was estimated from the results for the different configurations using different values for r_{max} (0.27–0.29 nm). The Z_{SiSi} determined from fits to $N(r)$ are in reasonable agreement with Z_{SiSi} determined using the RMC method (see table 4). The error in Z_{SiSi} determined from the fits to $S(\kappa)$ is large because of the strong correlation between the fitting parameters.

The Z_{SiSi} from the fits to $S(\kappa)$ show the same concentration and temperature dependence as Z_{SiSi} determined with the RMC method. In figure 7 we show Z_{SiSi} determined using these three methods, Z_{SiSi} of the intermediate solid phases and Z_{SiSi} of an AIMD simulation of liquid $Li_{12}Si_7$ [11]. We find that Z_{SiSi} in the liquid state has a similar concentration dependence to that in the solid state. The concentration dependence of Z_{SiSi} in liquid Li–Si is in agreement with the assumption made by Meijer *et al* [4] that poly-anions are present in the liquid state.

In figure 8 we show a two-dimensional projection of the three-dimensional structure of $Li_{80}Si_{20}$ and $Li_{57}Si_{43}$ at 888 K. Solid lines are drawn between Si atoms if they are separated by less than 0.28 nm. We find that the number of lines strongly increases at increasing Si concentration. In $Li_{80}Si_{20}$ we find that Si atoms are either isolated or they form Si dumbbells. In the Si-rich alloys, $Li_{65}Si_{35}$ and $Li_{57}Si_{43}$, three-dimensional clusters containing twofold-, threefold-, and fourfold-coordinated Si atoms are formed. This is similar to the results of the AIMD simulation of liquid $Li_{12}Si_7$ [11].

It is interesting to compare Li–Si with Li–Pb [19] in order to study the effect of the size of the post-transition group IV element. Meijer *et al* [4] pointed out that replacing Pb by Si enlarges the electronegativity difference and reduces the size of the anion, favouring covalent bonding. This does indeed occur in $Li_{65}Si_{35}$ and $Li_{57}Si_{43}$. However, the structure of liquid $Li_{80}Si_{20}$ is qualitatively very similar to the structure of liquid $Li_{80}Pb_{20}$. The Pb–Pb partial pair correlation function has a broad peak at a distance which is close to the distance of maximum separation between Pb atoms. The Li–Pb partial pair correlation function has a sharp first maximum and the first maximum of $g_{LiLi}(r)$ of Li_4Pb is broad. Copestake *et al* [27] showed that the structure of liquid $Li_{80}Pb_{20}$ can be modelled reasonably well

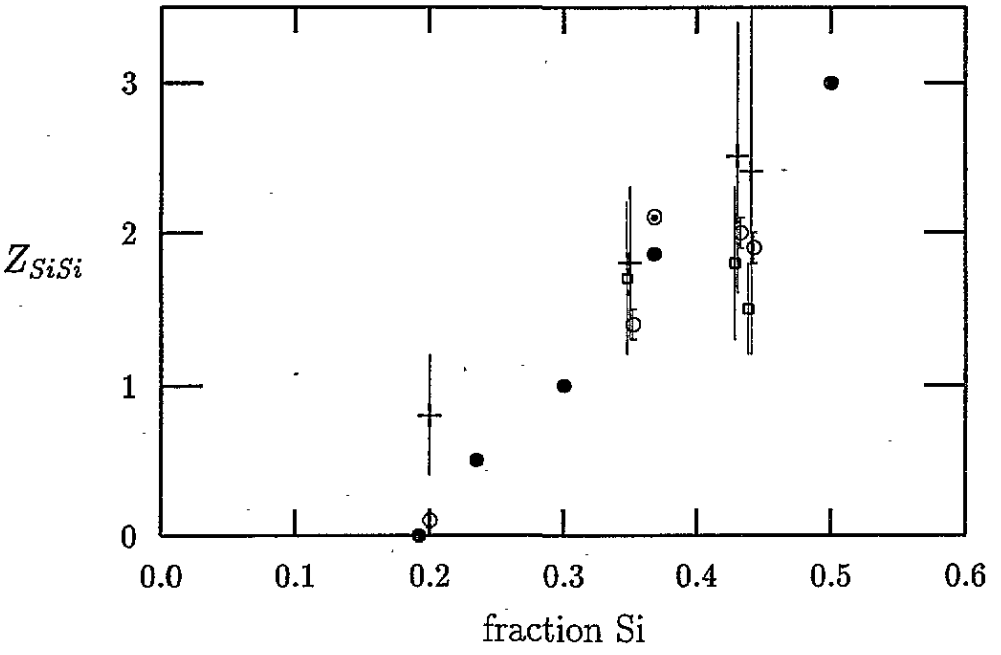

Figure 7. Z_{SiSi} for liquid Li–Si determined using different methods. Plusses: from $S(\kappa)$; squares: from $N(r)$; circles: RMC results; dots: solid-state phases; circle plus dot: AIMD result for liquid $Li_{12}Si_7$ [11]. The results for $Li_{57}Si_{43}$ at 1073 K have been shifted by +0.01 with respect to the results for $Li_{57}Si_{43}$ at 888 K. The results from fits to $N(r)$ and from the RMC modelling have been shifted by −0.002 and +0.002, respectively.

by pairwise potentials. This was possible because they assumed that the alloy is partially ionic and because $S(\kappa)$ of $Li_{80}Pb_{20}$ reflects directly $S_{CC}(\kappa)$. The latter allowed for the determination of one of the parameters of the model potential from experimental data. It might be possible to apply the same approach to the Li-rich alloy $Li_{80}Si_{20}$ because of the similarities between the partial structure factors of $Li_{80}Si_{20}$ and $Li_{80}Pb_{20}$, and because $S(\kappa)$ of $Li_{80}Si_{20}$ is dominated by $S_{CC}(\kappa)$. The larger difference in electronegativity for Li–Si (1.85 V) with respect to Li–Pb (1.25 V) might enhance the ionic character of $Li_{80}Si_{20}$.

A comparison of the AIMD results for liquid KSi with the present results for Li–Si enables us to study the effect of the size of the alkali atom on the structure. $g_{SiSi}(r)$ of KSi is qualitatively very similar to $g_{SiSi}(r)$ of $Li_{65}Si_{35}$ and $Li_{57}Si_{43}$. Si in KSi is also present in an extended network with twofold-, threefold-, and fourfold-coordinated sites. A quantitative comparison of Z_{SiSi} of KSi with our results for Z_{SiSi} is not useful because Z_{SiSi} in liquid Li–Si is strongly dependent on the concentration.

The structure of liquid Li–Ga alloys was studied by neutron diffraction [28] and by molecular dynamics simulation [29]. The picture of the liquid structure is one of Ga clusters, which resemble broken pieces of the Ga structure in the solid phases, embedded in a matrix of randomly close-packed Li atoms. The Li–Ga alloys also show a tendency for hetero-coordination. The main difference between Li–Si and Li–Ga is the covalent character of Si in the Si-rich alloys of Li–Si which is favoured by the small size of the anion and the large electronegativity difference (1.85 V for Li–Si and 1.25 for Li–Ga).

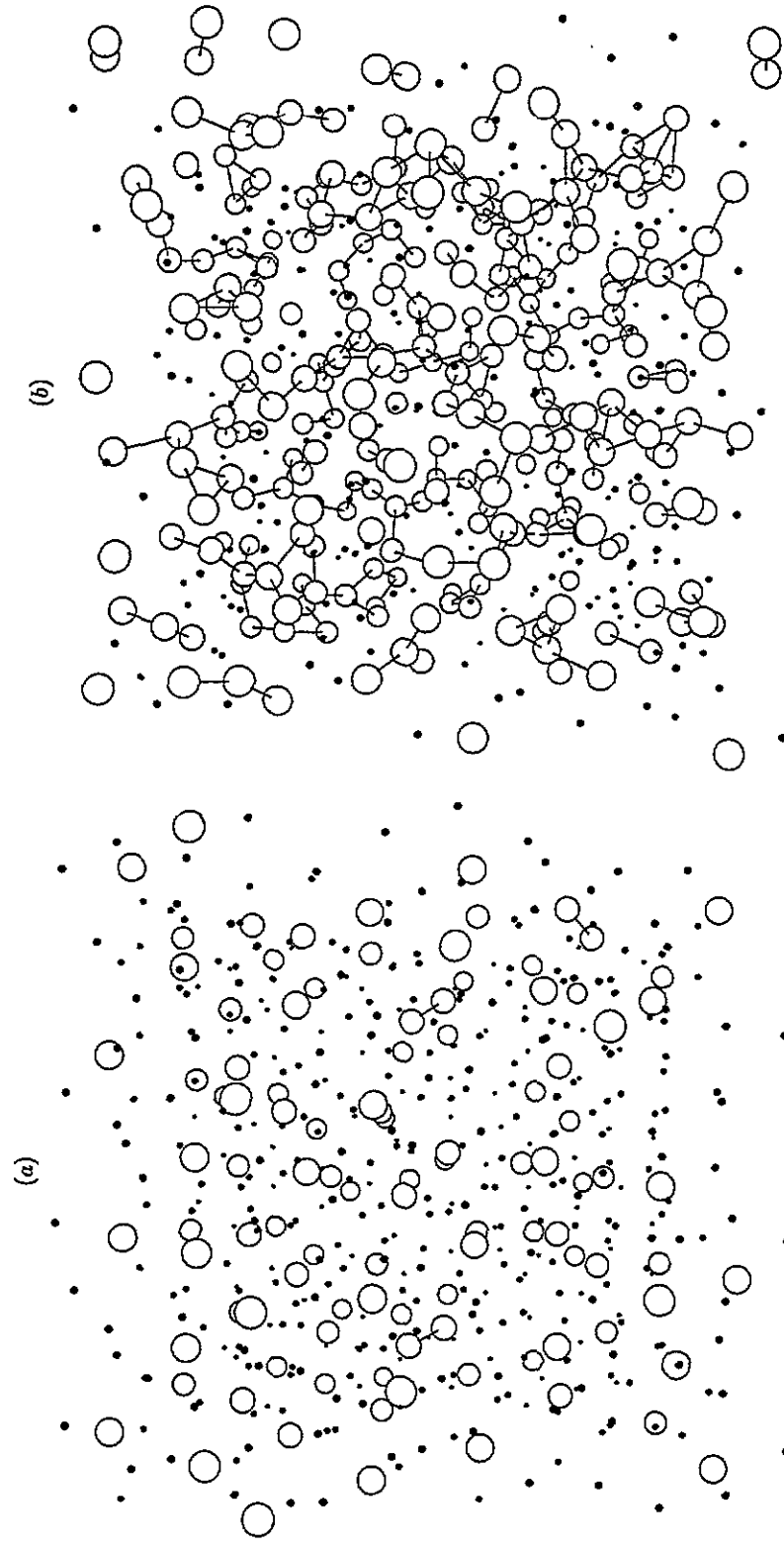

Figure 8. Two-dimensional projection of the three-dimensional structure of $Li_{80}Si_{20}$ (*a*) and $Li_{57}Si_{43}$ at 888 K (*b*). Circles: Si atoms; dots: Li atoms. The solid lines connect Si atoms that are separated by less than 0.28 nm, the position of the first minimum of $g_{SiSi}(r)$ in $Li_{57}Si_{43}$.

5. Summary

The $S(\kappa)$ of the alloys under investigation are equal to (for $Li_{65}Si_{35}$) or dominated by the Bhatia–Thornton partial structure factor $S_{CC}(\kappa)$. We observe strong chemical ordering in all four $S(\kappa)$s. We have analysed the data by fitting models to $S(\kappa)$ and the radial distribution function $N(r)$, and by applying the reverse Monte Carlo method.

A fit with an intramolecular form factor to the large-κ part of $S(\kappa)$ shows that a well defined Si–Si distance, about 0.238 nm, occurs in the liquid state of the Si-rich alloys, $Li_{65}Si_{35}$ and $Li_{57}Si_{43}$. This distance is close to the interatomic distance between covalently bonded Si in solid Li–Si. The positive first peak and a negative second peak of the pair correlation functions $g(r)$ of $Li_{65}Si_{35}$ and $Li_{57}Si_{43}$ indicate the preference for a self-coordination and a hetero-coordination, respectively. The positions of the first maxima in $g(r)$ of $Li_{65}Si_{35}$ and $Li_{57}Si_{43}$ agree well with the distance between covalently bonded Si in the solid state. The positive peak is absent in $g(r)$ of $Li_{80}Si_{20}$. We have fitted the first maximum and the first minimum of $N(r)$ of $Li_{65}Si_{35}$ and $Li_{57}Si_{43}$ with two Gaussians and the first minimum of $N(r)$ of $Li_{80}Si_{20}$ with a single Gaussian. The position of the first Gaussian of $Li_{65}Si_{35}$ and $Li_{57}Si_{43}$ is close to the distance between covalently bonded Si in solid Li–Si. The minimum in $g(r)$ of the three alloys clearly indicates the preference for a hetero-coordination.

We used different and extreme starting configurations for the RMC modelling of $Li_{80}Si_{20}$. We obtain good agreement with the experimental $S(\kappa)$. We compare the RMC results for $Li_{80}Si_{20}$ with RMC results for $Li_{65}Si_{35}$ and $Li_{57}Si_{43}$ [25, 26]. $g_{SiSi}(r)$ of $Li_{80}Si_{20}$ does not have a sharp maximum close to the distance between covalently bonded Si in solid Li–Si. This differs from the results of the RMC modelling of $Li_{65}Si_{35}$ and $Li_{57}Si_{43}$. We find that the positions of the first peaks of $g_{LiLi}(r)$ and $g_{LiSi}(r)$ in $Li_{80}Si_{20}$ are close to the interatomic distances in solid $Li_{21}Si_5$ and $Li_{14}Si_6$.

We have determined the Si–Si partial coordination number Z_{SiSi} of the alloys in three ways: from fits to $S(\kappa)$ and to $N(r)$, and with the RMC method. The agreement between the RMC values and the values extracted from $N(r)$ is reasonable. The Z_{SiSi} cannot accurately be determined from the fits to $S(\kappa)$ using an intramolecular form factor because of the strong correlation between the fitting parameters. However, they do show the same concentration and temperature dependence as Z_{SiSi} determined with the RMC method. Z_{SiSi} in the liquid state has a similar concentration dependence to that in the solid state. The RMC modelling indicates that Si in $Li_{80}Si_{20}$ is either present in isolated Si atoms or in Si dumbbells. In the Si-rich alloys, $Li_{65}Si_{35}$ and $Li_{57}Si_{43}$, Si is present in a variety of poly-anions ranging from isolated Si atoms to large three-dimensional clusters which can contain twofold-, threefold-, and fourfold-coordinated Si atoms.

We have determined the Li–Si partial coordination number Z_{LiSi} in two ways: from $N(r)$ and from $g_{LiSi}(r)$ generated with the RMC method. The results from both methods are in good agreement. We find that the Z_{LiSi} of all the three alloys differs by about 15–20% from Z_{LiSi} in a random configuration. This is similar to what is found for liquid Li_4Pb where this difference is 25%.

The structure of $Li_{80}Si_{20}$ is qualitatively very similar to the structure in the 'ionic liquid' $Li_{80}Pb_{20}$. At decreasing Li concentration Si forms poly-anions. The poly-anions in $Li_{57}Si_{43}$ do not dissociate when the temperature increases by 185 K. The results from the AIMD simulation of liquid $Li_{12}Si_7$ are in good agreement with our results for $Li_{65}Si_{35}$ (e.g. $g_{SiSi}(r)$, Z_{LiSi}, Z_{SiSi}, Si structure). $g_{SiSi}(r)$ in liquid KSi (AIMD simulations [23]) is qualitatively very similar to $g_{SiSi}(r)$ in the Si-rich alloys. Si in KSi also forms a three-dimensional network with twofold-, threefold-, and fourfold-coordinated Si atoms.

The concentration dependence of Z_{SiSi} is in agreement with the assumption made by Meijer *et al* [4] that poly-anions are formed in the liquid state.

Acknowledgments

PdJ, PV, LdG and WvdL acknowledge the financial support from the Nederlandse Organisatie voor Wetenschappelijk Onderzoek NWO and from the EC Science plan (SC1*CT91-0754). The authors acknowledge fruitful discussions with G A de Wijs (University of Groningen).

References

[1] van der Lugt W 1991 *Phys. Scr.* T **39** 372
[2] Miedema A R, de Châtel P F and de Boer F R 1980 *Physica* B **100** 1
[3] Xu R and van der Lugt W 1991 *Physica* B **173** 435
[4] Meijer J A, van der Marel C, Kuiper P and van der Lugt W 1989 *J. Phys.: Condens. Matter* **1** 5283
[5] Evers J, Oehlinger G and Sextl G 1993 *Angew. Chem. Int. Edn Engl.* **32** 1442
[6] Nesper R, von Schnering H G and Curda J 1986 *Chem. Ber.* **119** 3576
[7] von Schnering H G, Nesper R, Tebbe K F and Curda J 1980 *Z. Metallk.* **71** 357
[8] Frank U, Müller W and Schäfer H 1975 *Z. Naturf.* b **30** 10
[9] Nesper R and von Schnering H G 1987 *J. Solid State Chem.* **70** 48
[10] Verkerk P, Ahda S, de Jong P H K and Kinderman R 1992 *Developments in the Physics of Fluids* ed W S Howells and A K Soper (Bristol: Hilger) F241
[11] de Wijs G A, Pastore G, Selloni A and van der Lugt W 1993 *Phys. Rev.* B **48** 13459
[12] van der Marel C, Vinke G J B and van der Lugt W 1985 *Solid State Commun.* **54** 917
[13] Boland B C 1990 RAL-90-041 *User Guide* Rutherford Appleton Laboratory
[14] Sears V F 1986 *Methods of Experimental Physics, Neutron Scattering Part A* vol 23, ed K Sköld and D L Price (Orlando, FL: Academic) p 533
[15] Soper A K, Howells W S and Hannon A C 1989 Analysis of time-of-flight diffraction data from liquid and amorphous samples *Rutherford Appleton Laboratory Report* RAL-89-046
[16] Howe M A, McGreevy R L and Howells W S 1989 *J. Phys.: Condens. Matter* 1 3433
[17] Ashcroft N W and Langreth D C 1967 *Phys. Rev.* **156** 685
[18] Bhatia A B and Thornton D E 1970 *Phys. Rev.* B **2** 3004
[19] Ruppersberg H and Egger H 1975 *J. Chem. Phys.* **63** 4095
[20] Harris R and Lewis L J 1983 *J. Phys. F: Met. Phys.* **13** 1359
[21] Egelstaff P A and Page D I 1971 *Mol. Phys.* **20** 881
[22] Dore J C 1984 *Molecular Liquids, Dynamics and Interactions* ed A J Barnes, W J Orville-Thomas and J Yarwood (Dordrecht: Reidel) p 383
[23] Galli G and Parrinello M 1991 *J. Chem. Phys.* **95** 7504
[24] McGreevy R L, Howe M A, Keen D A and Clausen K N 1990 *Neutron Scattering Data Analysis (IOP Conference Ser. 107)* (Bristol: Institute of Physics Publishing) p 165
[25] de Jong P H K, Verkerk P, van der Lugt W and de Graaf L A 1993 *J. Non-Cryst. Solids* **156–158** 978
[26] de Jong P H K and Verkerk P 1993 *Methods in the Determination of Partial Structure Factors* ed J B Suck, P Chieux, D Raoux and C Riekel (London: World Scientific) p 233
[27] Copestake A P, Evans R, Ruppersberg H and Schirmacher W 1983 *J. Phys. F: Met. Phys.* **13** 1993
[28] Reijers H T J, van der Lugt W, van Tricht J B, Vlak W A H M and Howells W S 1989 *J. Phys.: Condens. Matter* **1** 8609
[29] Hafner J and Jank W 1991 *Phys. Rev.* B **44** 11 662
[30] Ramirez R, Nesper R and von Schnering H G 1986 *Z. Naturf.* a **41** 1267